Crystal Structures of Substrate-Free and Retinoic Acid-Bound Cyanobacterial Cytochrome P450 CYP120A1[†,‡]

Karin Kühnel,[§,||] Na Ke,[⊥] Max J. Cryle,[§] Stephen G. Sligar,[#,+] Mary A. Schuler,[#,@] and Ilme Schlichting*[,§]

Department of Biomolecular Mechanisms, Max Planck Institute for Medical Research, Jahnstrasse 29, 69120 Heidelberg, Germany, and Departments of Microbiology, Biochemistry, Chemistry, Cell and Developmental Biology, and Plant Biology, University of Illinois, Urbana, Illinois 61801

Received February 26, 2008; Revised Manuscript Received April 22, 2008

ABSTRACT: The crystal structures of substrate-free and all-*trans*-retinoic acid-bound CYP120A1 from *Synechocystis* sp. PCC 6803 were determined at 2.4 and 2.1 Å resolution, respectively, representing the first structural characterization of a cyanobacterial P450. Features of CYP120A1 not observed in other P450 structures include an aromatic ladder flanking the channel leading to the active site and a triple-glycine motif within SRS5. Using spectroscopic methods, CYP120A1 is shown to bind 13-*cis*-retinoic acid, 9-*cis*-retinoic acid, and retinal with high affinity and dissociation constants of less than 1 μM. Metabolism of retinoic acid by CYP120A1 suggests that CYP120A1 hydroxylates a variety of retinoid derivatives in vivo. On the basis of the retinoic acid-bound CYP120A1 crystal structure, we propose that either carbon 2 or the methyl groups (C16 or C17) of the β-ionone ring are modified by CYP120A1.

Cytochrome P450 monooxygenases are ubiquitous heme-containing enzymes that catalyze the hydroxylation of nonactivated hydrocarbon bonds, epoxidation, dealkylation, and dehydrogenation reactions, among others (*1–4*). Cytochrome P450s are involved in many metabolic pathways, including the biosynthesis of lipids, steroids, fat-soluble vitamins, and antibiotics, and are of medical interest because they play a crucial role in the degradation of drugs and xenobiotics (*5–9*).

Existing in all kingdoms of life, more than 7000 genes encoding P450s[1] have been identified (http://drnelson.utmem.edu/CytochromeP450.html). As of the beginning of 2008, coordinates for 39 unique cytochrome P450 structures had been deposited in the Protein Data Bank. Despite this large number of structures, it is still a major challenge to deduce the function of a particular P450 enzyme from its sequence. The existing collection of P450 structures defined by crystallography and refined P450 alignment techniques (*10*) have made it possible to generate homology models for many previously uncharacterized P450s (*11*). The range of crystal structures now being determined will certainly improve these models and allow in silico screening procedures to narrow the range of potential substrates for novel P450s. Using these types of approaches, retinoic acid (RA) was proposed as a potential substrate of CYP120A1 from *Synechocystis* sp. PCC 6803, the first cyanobacterial P450 to be cloned, purified, and characterized (*12*). In this earlier analysis, addition of RA caused a shift in the Soret band to 389 nm that is indicative of a low-spin to high-spin transition of the iron, proving that RA does indeed bind in the active site (*12*).

Members of the CYP120 family occur not only in *Synechocystis* but also in other cyanobacteria, for example, CYP120A3 and CYP120D1 in *Cyanothece* sp. CCY0110, CYP120A4 in *Lyngbya* sp. PCC 8106, CYP120A5 in *Nodularia spumigena* CCY 9414, CYP120B1 and CYP120C1 in *Nostoc punctiforme* PCC 73102, and CYP120A2 and CYP120E1 in *Trichodesmium erythraeum* IMS101. The existence of this P450 gene in cyanobacteria is independent of the ecotype and cellular organization of their hosts. For example, *Synechocystis* and *Nostoc* grow in freshwater habitats, while *Nodularia* is commonly found in seawater. *Nostoc* is a filamentous, nitrogen-fixing cyanobacterium, whereas *Synechocystis* is a unicellular and non-nitrogen-fixing organism.

Here, we describe the CYP120A1 crystal structure in its substrate-free and all-*trans*-retinoic-acid bound states. Experimental evidence indicating that RA is modified by CYP120A1 is presented, with the structure suggesting that this occurs either at C2 or at one of the methyl groups (C16 or C17) on the β-ionone ring. We show spectroscopically that CYP120A1 protein can bind all-*trans*-retinoic acid, 13-*cis*-retinoic acid, 9-*cis*-retinoic acid, retinal, and 13-*cis*-β-

[†] This work was supported by the Deutsche Forschungsgemeinschaft SFB 623 (I.S.) and National Institutes of Health Grants R01 GM071826 (M.A.S.) and R37 GM31756 and R01 GM33775 (S.G.S.).

[‡] Coordinates and structure factors have been deposited in the Protein Data Bank as entries 2ve3 and 2ve4.

* To whom correspondence should be addressed. E-mail: ilme.schlichting@mpimf-heidelberg.mpg.de. Telephone: +49 6221 486 500. Fax: +49 6221 486 585.

[§] Max Planck Institute for Medical Research.

[||] Present address: Department of Neurobiology, Max Planck Institute for Biophysical Chemistry, Am Fassberg 11, 37077 Göttingen, Germany.

[⊥] Department of Microbiology, University of Illinois.

[#] Department of Biochemistry, University of Illinois.

[+] Department of Chemistry, University of Illinois.

[@] Department of Cell and Developmental Biology and Department of Plant Biology, University of Illinois.

[1] Abbreviations: CYP120A1, cytochrome P450 from *Synechocystis* sp. PCC 6803; K_d, dissociation constant; PDB, Protein Data Bank; PEG, polyethylene glycol; P450, cytochrome P450; RA, retinoic acid; SRS, substrate recognition site.

10.1021/bi800328s CCC: $40.75
Published on Web 05/31/2008

Table 1: Data Collection and Refinement Statistics

	substrate-free CYP120	RA-bound CYP120
PDB entry	2ve4	2ve3
space group	*C*2	*C*2
unit cell dimensions *a*, *b*, *c* (Å)	153.6, 122.2, 64.9 (β = 115.0°)	141.5, 133.0, 67.4 (β = 114.5°)
beamline	SLS X10SA	SLS X10SA
wavelength (Å)	0.9791	1.0007
resolution of data (Å) (high-resolution bin)	20−2.4 (2.40−2.46)	20−2.1 (2.10−2.15)
no. of observations/no. of unique reflections	211009/40633	184206/62855
completeness (%), total (high)	95.5 (80.3)	95.0 (90.1)
$I/\sigma I$, total (high)	11.6 (3.1)	9.6 (3.8)
R_{sym}[a] (%), total (high)	7.7 (46.2)	9.9 (42.3)
Wilson *B* factor (Å^2)	58.1	32.6
	Refinement	
R_{work}[b] (%)/R_{free}[c] (%)	23.0/30.4	22.3/26.7
residues included in the model (total no. of protein atoms)	A11−A441, B11−B442 (6897)	A9−A443, B10−B163, B167−B287, B292−B443 (6891)
water molecules	161	303
ligands (total no. of atoms)	two hemes (86)	two hemes (86), two RAs (44)
overall *B* factor (Å^2)	56.8	28.0
root-mean-square deviation for bond lengths (Å)	0.012	0.010
root-mean-square deviation for bond angles (deg)	1.44	1.37

[a] $R_{sym} = \sum|I - \langle I\rangle|/\sum I$. [b] $R_{work} = \sum||F_{obs}| - k|F_{calc}||/\sum|F_{obs}|$. [c] The calculation of R_{free} involved 5% of randomly chosen reflections.

carotene, suggesting that the character and position of the substrate fatty acid chains are quite flexible in the catalytic site. Implications for the biological function of CYP120A1 are discussed.

MATERIALS AND METHODS

Substrate Binding Spectra. CYP120A1 from *Synechocystis* sp. PCC 6803 was expressed and purified as described previously (*12*). UV−visible absorption spectra were obtained by using a Cary 300 Bio ultraviolet−visible spectrometer with a scan rate of 120 nm/min. All-*trans*-retinal, 9-*cis*-retinoic acid, and 13-*cis*-retinoic acid were purchased from Sigma (St. Louis, MO), and 10 mM stock solutions of each compound were made in ethanol. Binding assays were performed by spectrometric titration of 1−2 μM CYP120A1 protein in 200 mM NaCl, 20 mM sodium phosphate (pH 7.4) buffer with increasing amounts of the retinoid stock solutions. Difference spectra were monitored in tandem cuvettes.

Due to the high affinity of CYP120A1 for these three retinoids, the substrate binding data were fit using Matlab to the following quadratic equation from Segel (*13*) that takes into account the amount of enzyme in the enzyme−substrate complex at each point of the titration:

$$\Delta A = (\Delta A_{max}/2E_t)\{S + E_t + K_d - [(S + E_t + K_d)^2 - 4SE_t]^{0.5}\}$$

where ΔA equals $A_{388} - A_{418}$, S is the substrate concentration, E_t is the total enzyme concentration, and K_d is the observed dissociation constant.

Crystallization. Selenomethionine CYP120A1 was prepared by expressing the protein in *Escherichia coli* cells grown in minimal medium supplemented with selenomethionine (*14*). The labeled protein was purified as the native protein but in the presence of 10 mM β-mercaptoethanol. Substrate-free selenomethionine CYP120A1 crystals were grown with the hanging drop method in Linbro plates at 4 °C with 1 μL of 15 mg/mL CYP120A1 in 0.15 M NaCl and 30 mM HEPES (pH 7.4) mixed with 0.25 μL of 1.5 mM *O*-tetradecylphosphorylcholine (Sigma) and 1 μL of reservoir solution containing 5% ethylene glycol, 7% PEG 3350, and 0.1 M Tris (pH 7.5). Rodlike crystals (100 μm × 50 μm × 30 μm) grew within 2 weeks. They were flash-cooled in liquid nitrogen after being transferred into a cryoprotectant consisting of 25% ethylene glycol, 7% PEG 3350, and 0.1 M Tris (pH 7.5).

CYMAL-6 from Hampton Research (Aliso Viejo, CA) was required for the crystallization of RA-bound CYP120A1. The detergent was first mixed with the native protein at a concentration of 1.1 mM. A freshly prepared saturated retinoic acid (Fluka) stock solution in dimethyl sulfoxide (130 mM) was added stepwise, and complex formation was followed spectroscopically with a Soret band peak shift from 418 to 389 nm observed upon binding of retinoic acid (*12*). Spectra were recorded with an ND-1000 spectrophotometer (NanoDrop Technologies Inc., Rockland, ME) at 20 °C.

RA-bound CYP120A1 crystals were grown by sitting drop vapor diffusion in 96-well low-profile Greiner microplates with 100 nL of reservoir solution containing 1.2 M potassium sodium tartrate and 0.1 M MES (pH 6.5) added to 100 nL of 15 mg/mL RA-bound CYP120A1 and 1.1 mM CYMAL-6 using a Mosquito robot (TTP Labtech, Royston, England). Crystals grew within 2 weeks at 4 °C in the dark and were then transferred into a RA-saturated cryoprotectant solution containing 20% glycerol, 1.1 M potassium sodium tartrate, and 70 mM MES (pH 6.5) and flash-cooled in liquid nitrogen.

Data Collection and Structure Determination. Diffraction data of cryo-cooled crystals kept at 90 K were collected on beamline X10SA (SLS). Data processing and scaling were carried out with the XDS software package (*15*) as shown in Table 1. Molecular replacement attempts with various P450 structures were without success, and a SAD data set was collected from a selenomethione-labeled, substrate-free CYP120A1 crystal. Initially, data were indexed in orthorhombic space group *I*222 (a = 65.0 Å, b = 122.3 Å, and c = 139.3 Å) with one molecule in the asymmetric unit. Six Se sites and the position of the iron, which also shows an anomalous signal at the selenium absorption wavelength, were identified with HKL2MAP (*16*). Phasing was done with SHARP (overall FOM acentric/centric, 0.28/0.15) and yielded an interpretable electron density map (*17*). Automated model

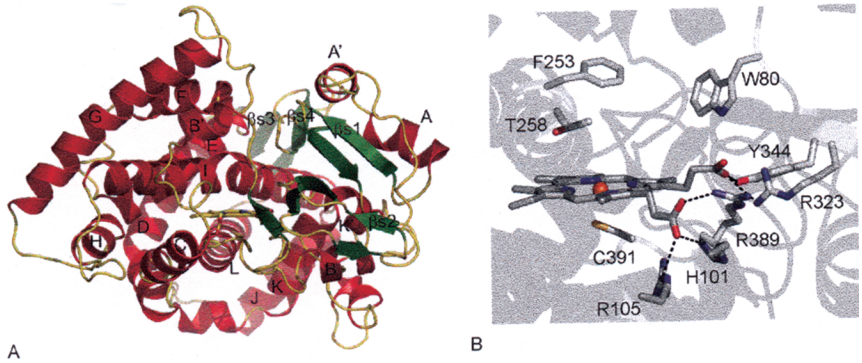

FIGURE 1: (A) Overall structure of CYP120. (B) Close-up of the active site of substrate-free CYP120. Residues interacting with the heme propionate groups are shown. Phe253 and Trp80 restrict access to the active site on the distal side. Hydrogen bonds and salt bridges between the heme propionate group and neighboring amino acids are indicated with dotted lines.

building with Resolve (*18*) gave a model containing 197 of 444 residues. The graphics program Coot (*19*) was used for manual rebuilding and completion of the model. Refinement was carried out with Refmac5 (*20*). However, R_{free} remained high at approximately 36%, although the model was more than 90% complete. The cumulative intensity distributions calculated with the CCP4 program TRUNCATE (*21, 22*) indicated no twinning of the data. The data were then reprocessed in lower-symmetry space group *C*2 with two molecules in the asymmetric unit, which resulted in better electron density maps, and R/R_{free} continued to decrease during refinement (final statistics are listed in Table 1). The structure of RA-bound CYP120A1 was determined by molecular replacement with Molrep (*23*) in space group *C*2, using the substrate-free CYP120A1 structure as a search model. Figures were prepared with Pymol (DeLano Scientific LLC, San Carlos, CA).

RESULTS

Overall Structure. The structure of CYP120A1 determined at a resolution of 2.4 Å (Table 1) has a characteristic P450 fold consisting of 16 α-helices and 11 β-strands, which are arranged in four β-sheets (Figure 1A). The core of the protein is formed by a four-helix bundle composed of helices D, E, I, and L with the heme group sandwiched between helices I and L and linked to the protein via Cys391. The propionate side chains of the heme interact with the protein through hydrogen bonds to His101 and Tyr344 and form salt bridges with Arg323, Arg389, and Arg105 (Figure 1B).

The distal side of the heme is hydrophobic, similar to other P450s. Two aromatic residues, Phe253 and Trp80, gate access to the heme. Of these, Trp80 is part of the loop preceding helix B′ that is contained within SRS1 [substrate recognition site 1 (*32*)], a highly variable region found to be important for substrate recognition and binding (*24*). Phe253 is part of helix I, which stretches along the length of the catalytic site, and is located prior to ^{254}AGHET^{258}, which is a helix I signature motif. In the substrate-free structure, helix I displays a helical distortion at Gly255, which is often observed in P450s due to the disruption of the normal α-helical hydrogen bonding pattern between the carbonyl oxygen of residue *i* and the amide nitrogen of residue *i* + 4 (*25, 26*). Instead, a hydrogen bond is formed between the carbonyl oxygen of Ala254 and the hydroxyl group side chain of the highly conserved Thr258 in CYP120A1.

A water molecule, 5 Å from the iron, is observed on the distal heme side of the substrate-free structure. Although the distal cavity is filled with water, no other ordered water molecules above the heme are visible in the electron density map. This is not unexpected since the substrate binding pocket is hydrophobic, allowing it to accommodate the nonpolar RA molecule.

We also did not observe a water coordinated to the iron, likely due to a photoreduction of the hexacoordinated ferric iron to the pentacoordinated ferrous state, which rapidly occurs during data collection at synchrotron X-ray sources as recently demonstrated for the heme-thiolate enzyme chloroperoxidase (*27*).

A search of the PDB with DALI (*28*) revealed *Bacillus megaterium* P450BM3 (PDB entry 2HPD) (*29*), which is a fatty acid hydroxylase, as the closest structural homologue of CYP120A1. Other similar structures are fatty acid peroxygenase P450BSβ from *Bacillus subtilis* (1IZO) (*30*) and *Thermus thermophilus* CYP175A1 (1WIY). CYP120A1 and P450BM3 have 21% identical sequence, and the Cα backbones of the two structures superimpose with a root-mean-square deviation (rmsd) of 2.5 Å. To investigate whether CYP120A1 might also bind fatty acids, *N*-palmitoylglycine, a substrate of P450BM3 (*31*), was added to CYP120A1, but no Soret peak shift from 418 to 389 nm characteristic for a low-spin to high-spin transition was observed. Therefore, *N*-palmitoylglycine has been excluded as a substrate for CYP120A1.

While structural diversity in their catalytic sites provides individual members of the P450 superfamily with different specificities, all must maintain a conserved mechanism of catalysis and prevent unregulated solvent access. These requirements, in addition to the restrictions imposed by the conserved P450 fold that surrounds extremely different substrates, are met by an induced fit mechanism. The enzymes have open and closed conformations depending on the absence or presence of substrate. However, the conformational equilibria between open and closed states differ between the various P450 family members. For instance, the open form exists only transiently in P450cam but is stable in other forms such as P450BM3 (*29*). P450BM3 also serves as the paradigm for conformational changes upon substrate binding. In the substrate-free state, P450BM3 adopts an open conformation with a wide substrate access channel (*29*), but in the presence of the substrate *N*-palmitoylglycine, helix B′, the N-terminal part, helices F and G, and the F−G loop,

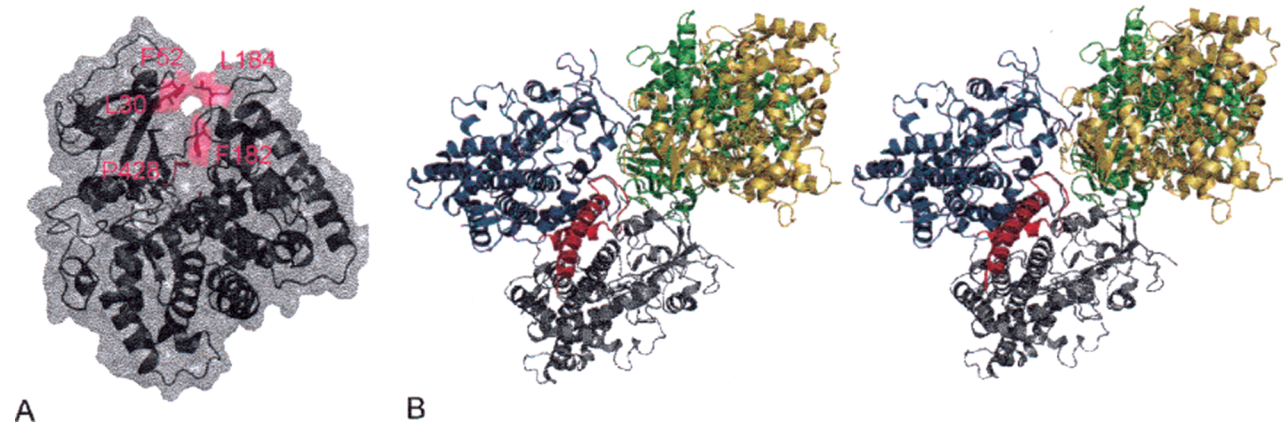

FIGURE 2: (A) Substrate-free crystal structure crystallized in a semiclosed conformation. This creates two bottlenecks for access of substrate to the active site. To allow binding of retinoic acid, CYP120A1 must adopt a more open conformation in solution at least transiently. (B) Crystal lattice contacts involve the F−G loop (red) and could stabilize the semiclosed conformation despite the absence of substrate, or alternatively, the half-closed state is stable due to hydrophobic contacts within the substrate channel, which caused the enzyme to crystallize in the conformation.

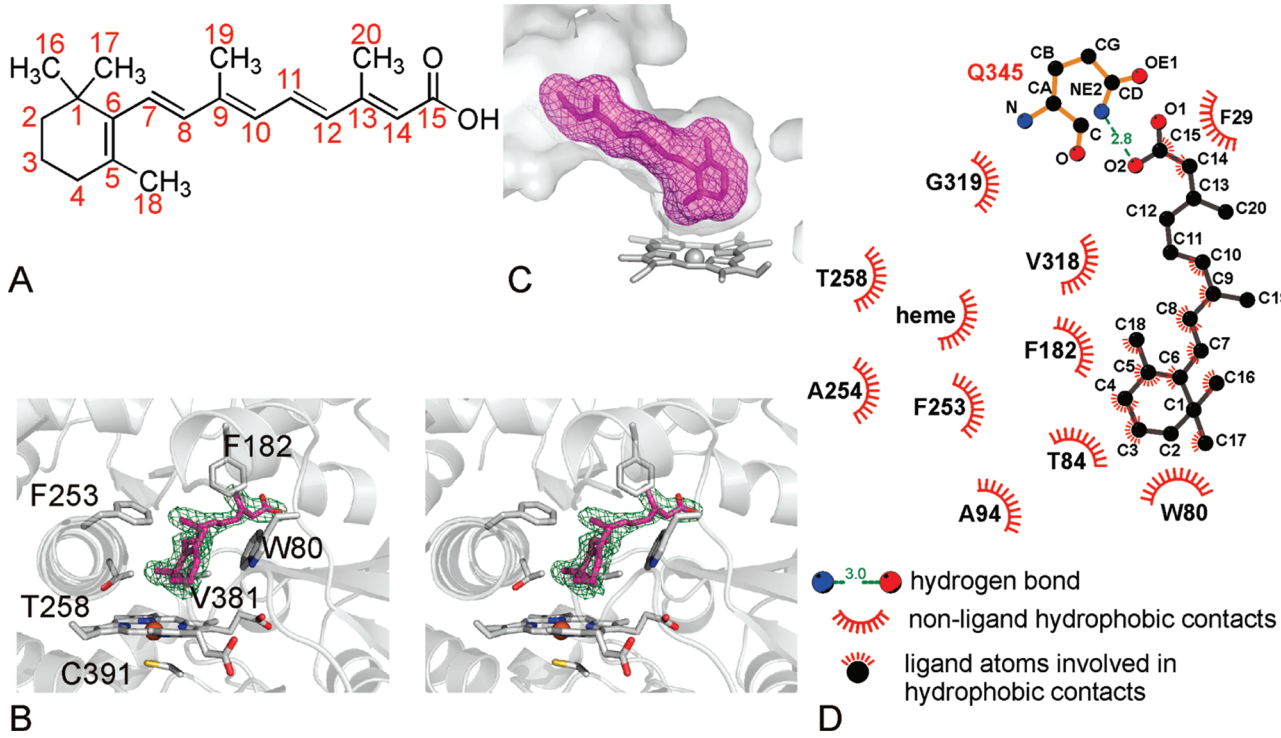

FIGURE 3: (A) Structure of retinoic acid. (B) Stereoview of the active site bound with RA. The SigmaA-weighted $mF_o - DF_c$ omit map is contoured at 2.5σ. (C) Surface representations of the active site and RA. A tight fit between RA and CYP120A1 is observed. Substrate binding seals the active site. (D) Schematic representation of the contacts between retinoic acid and CYP120A1 prepared with Ligplot (*44*).

which act as a lid, are moved in and seal the substrate binding pocket (*31*).

The channel allowing access of the substrate to the active site is structurally conserved and provided by movement of the helices B′, F, and G. It seems that this is also the case for CYP120A1, since access of RA to the active site is prevented by two bottlenecks. The distances among the side chains of residues Leu30 in helix A′, Phe52 located in the turn connecting strands 1 and 2 of β-sheet 1, and Leu184 in the F−G loop are only 4−5 Å, and the gap between Pro428 located in the hairpin region of β-sheet 4 and Phe182, also part of the F−G loop, is 5 Å (Figure 2A). RA cannot squeeze through these narrow gaps on its way to the active site. Therefore, helices F and G and the F−G loop must move such that the enzyme adopts a more open conformation for substrate binding. It is unclear whether the observation of a semiclosed conformation is caused by the equilibrium between open and closed forms in CYP120A1 being on the closed form, likely due to the hydrophobicity of the substrate channel or whether crystal contacts cause helices F and G and the F−G loop to interact (Figure 2B).

Retinoic Acid-Bound CYP120A1. RA (Figure 3A) was identified as a potential substrate through in silico docking using a homology model of CYP120A1 (*12*). To identify the interactions between the CYP120A1 protein and retinoic acid and, thus, understand the mode of metabolism of retinoic acid by CYP120A1, we determined the crystal structure of RA-bound CYP120A1. Since attempts to form the substrate complex by soaking unliganded crystals with substrate were unsuccessful, a preformed CYP120A1−retinoic acid complex

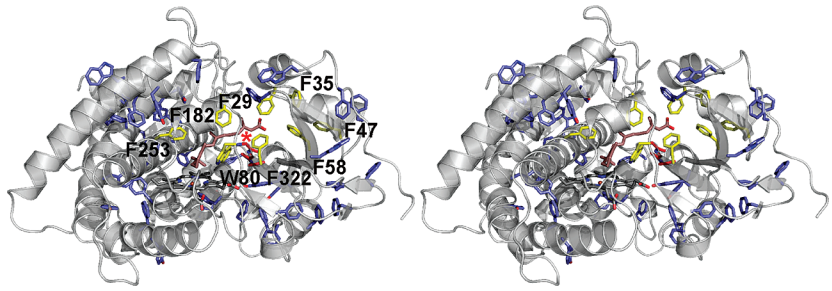

FIGURE 4: Clusters of aromatic amino acids spread throughout the molecule. Eight aromatic residues (yellow) form a ladder, which flanks the channel leading to the active site. These residues form a hydrophobic surface for binding of the hydrophobic tail of RA, while the β-ionone ring is sandwiched between Phe253 and Trp80. The Gly319-Gly320-Gly321 stretch (red) within SRS5 is marked with a red asterisk in this stereoview.

was crystallized instead. Convincing electron density for the substrate is visible above the hemes of both molecules in the asymmetric unit (Figure 3B).

In this structure, the β-ionone group binds in a tilted fashion at an angle of approximately 65° toward the heme plane. The nonpolar ring of RA is sandwiched between Trp80 and Phe253 with distances of approximately 4 Å to each side chain and is oriented parallel to the aromatic ring of Trp80. A snug fit between the substrate and CYP120A1 is observed (Figure 3C). Since RA is a very hydrophobic molecule, it interacts almost entirely through van der Waals contacts with CYP120A1. The only exception is a hydrogen bond, which is formed between the carboxyl group of RA and Gln345 (Figure 3D).

Aromatic clusters are distributed throughout the protein. A remarkable and unique feature of CYP120A1 is the ladderlike arrangement of a number of aromatic residues near the active site (Figure 4), providing a structural explanation for substrate binding. One "strand" accommodates Trp80, Phe322, Phe58, and Phe47, which face residues Phe253, Phe182, Phe29, and Phe35, respectively. The distances between the side chains from opposing strands are approximately 4 Å. These amino acids form a hydrophobic surface on which the isoprenoid tail of RA sits, while the β-ionone ring is sandwiched between Phe253 and Trp80. Another unique property of CYP120A1 is a triple-glycine stretch (residues 319−321) within SRS5 (*32*) (Figure 4). These residues are part of strand 4 from β-sheet 1 and the loop preceding it. More bulky amino acids at position 319 would clash with the isoprenoid group, and a substitution of Gly321 would cause a collision with the side chain of Trp80.

The substrate-free and RA-bound CYP120A1 crystal structures superimpose with a rmsd of 1.3 Å. For comparison, both molecules in the asymmetric unit of the substrate-free structure overlay with a rmsd of 0.3 Å, whereas the differences between the two molecules in the asymmetric unit of retinoic acid-bound CYP120A1 are larger, with a rmsd of 0.6 Å. The largest differences are observed in the F−G loop and the loop connecting helices J and K, which is also partially disordered in one of the two molecules in the substrate-bound structure (see Table 1).

A number of conformational changes are induced upon substrate binding. The F−G loop moves 2 Å closer to the active site (Figure 5A,C). In addition, helices A and A′ shift by approximately 4 Å toward the heme, pulling β-strands 1 and 2 of the large β-sheet 1 along (Figure 5A). These movements and RA, which acts as a plug, seal off the active site from the surrounding solvent. The most significant

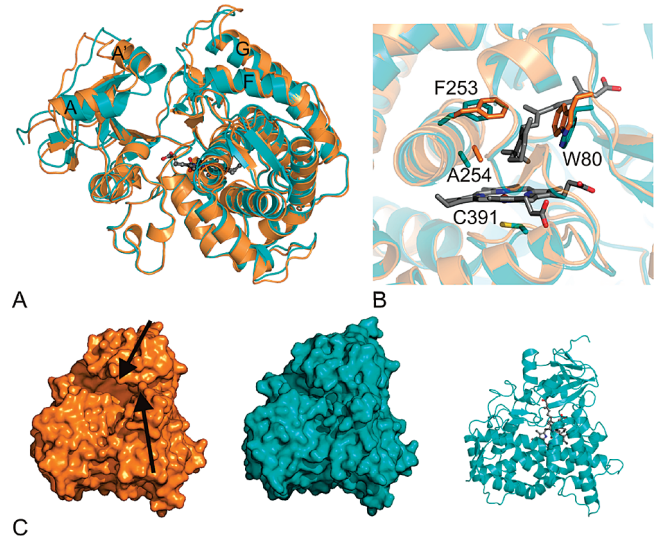

FIGURE 5: (A) Superimposition of substrate-free (orange) and RA-bound CYP120A1 (blue). (B) Comparison of active sites. Binding of RA induces a straightening of helix I. The aromatic side chain of Trp80 packs parallel to the β-ionone ring of RA. The substrate-free structure is colored orange and the complex blue. (C) Surface representations of the substrate-free structure (orange) and the RA-bound complex (blue). On the right, a ribbon representation of the molecule is shown in the same orientation. Upon binding of RA, the enzyme adopts a more closed conformation. Movements of the N-terminal part and the F−G loop are indicated by arrows.

conformational change in the active site is a straightening of helix I caused by the β-ionone ring pushing Ala254 and Phe253 aside (Figure 5B). No new ordered water molecules near the heme are observed in the substrate-bound structure, despite the changes in the active site and the higher resolution (2.1 Å) of the data compared to that of the substrate-free structure (2.4 Å).

On the basis of the modeled RA-bound CYP120A1 complex published previously (*12*), the reactive carbon was predicted to be the carbon atom on the β-ionone cycle located in a position para to the carbon linkage to the polyene chain of RA. Subsequent in vitro analysis of [^{3}H]retinoic acid incubated with purified *E. coli*-expressed CYP120A1 protein mixed with *Synechocystis* cell lysate identified a metabolite migrating between 4-hydroxyretinoic acid and 4-oxoretinoic acid standards on thin layer chromatography plates (see the Supporting Information, Figures S1−S3). These data, which exclude carbon 4 as the reaction site, are corroborated by the crystal structure, which shows carbon 4 pointing away from the active site with a carbon−iron distance of 7.2 Å. In contrast, the two methyl carbons, C16 and C17, of the

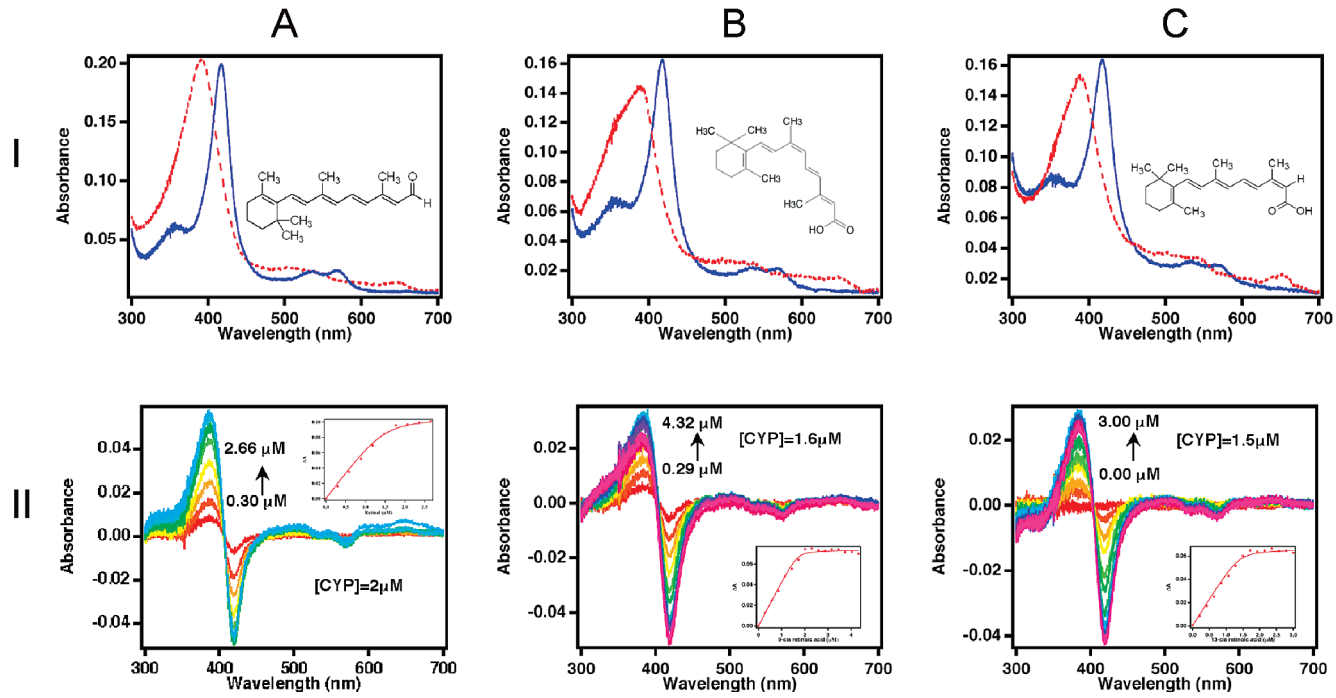

FIGURE 6: CYP120A1 substrate binding spectra. The top panels show binding of retinoids all-*trans*-retinal (A), 9-*cis*-retinoic acid (B), and 13-*cis*-retinoic acid (C) shifts CYP120A1 from low-spin (solid line) to high-spin (dotted line) states. The molecular structure of each retinoid appears at the top right of each panel. The bottom panels show type I difference spectra for CYP120A1 with each of these retinoids at increasing concentrations with the absorbance difference between 388 and 418 nm at each concentration plotted at the top right of each panel.

β-ionone ring are closest to the iron with distances of 4.4 and 4.5 Å, respectively, and carbon 2 is only slightly farther with a distance of 4.9 Å. These values are similar to the iron-reactive carbon distances (4−5 Å) observed in other P450 substrate complexes, such as P450cam (*33*), P450eryF (*34*), and P450epoK (*35*). When the heme of the CYP120A1 RA-bound structure is superimposed with the heme of the P450cam−oxygen complex (1DZ8) (*36*), the RA carbon closest to reactive camphor carbon 5 is retinoic acid carbon 2 with a distance of 0.7 Å. On the basis of this superimposition and the fact that secondary substituted carbons are more reactive than methyl carbons, it is likely that retinoic acid carbon 2 is hydroxylated by CYP120A1. However, we cannot completely exclude the possibility that one of the methyl groups might be modified.

Since the P450cam cyanide complex is a good mimic for the oxygen-bound state of this enzyme (*37*), we tried to generate a ternary cyanide−RA−CYP120A1 complex by soaking potassium cyanide into RA−CYP120A1 crystals, but no electron density fitting a cyanide molecule at the iron could be observed. This is consistent with data obtained from solution spectra in which addition of potassium cyanide to RA-bound CYP120A1 failed to produce a red shift of the Soret band (389 nm), indicating that no transition from a high-spin to low-spin state took place.

Retinoid Binding. Since RA is one of several possible carotenoid derivatives present in photosynthetic cyanobacteria, several related derivatives were analyzed for binding to CYP120A1. All-*trans*-retinal, 9-*cis*-retinoic acid, and 13-*cis*-retinoic acid bind effectively to the CYP120A1 protein, producing typical type I binding spectra indicative of low-spin to high-spin conversions (bottom panels in Figure 6). In these, the Soret band shifts from 417 to 391 nm for all-*trans*-retinal and 9-*cis*-retinoic acid (Figure 6A,B) or to 387 nm for 13-*cis*-retinoic acid (Figure 6C). Type I binding titrations at increasing concentrations of each substrate analyzed as described in Materials and Methods indicate that the binding affinity (K_d) for each of these retinoids is less than 1 μM, which is as tight as previously determined for all-*trans*-retinoic acid ($K_d = 0.74$ μM) (*12*). Thus, all-*trans*-retinal, 13-*cis*-retinoic acid, and 9-*cis*-retinoic acid are all likely to be metabolized by CYP120A1. Modeling of these three compounds, using the computational procedure described in ref *12*, in the catalytic site of the RA-bound CYP120A1 crystal structure (after deletion of the retinoic acid coordinates) indicates that bindings of retinoic acid, retinal, and apo-8′-carotenal are sterically and energetically allowed, with values of the scoring functions used that correspond to relatively tight predicted binding affinities. Comparison of the experimental and computational binding modes of retinal indicates that the computational approach nicely reproduces the experimental pose, in particular, the relative orientation of the heme atoms and atoms in the β-ionone cycle, despite the *cis* orientation of some dihedral angles in the polyene.

Similar modeling of the significantly longer all-*trans*-β-carotene in the RA-bound CYP120A1 structure indicates that this compound clashes with helix A′. This is consistent with experimental solution spectra showing that addition of carrot carotene mixtures containing β- and α-carotene (in a ratio of approximately 2:1) to CYP120A1 does not generate a Soret band shift (data not shown). In contrast, the 13-*cis*-β-carotene isomer can be fitted into the RA-bound CYP120A1 structure without major clashes, and after incubation for 2 days, a shoulder at 395 nm appeared on the Soret band indicating 13-*cis*-β-carotene binding (Figure S4). However, the relevance of a possible hydroxylation of 13-*cis*-β-carotene

by CYP120A1 is unclear (see the Supporting Information for a discussion).

DISCUSSION

RA is an important signaling molecule in more highly developed organisms and is involved in the control of cellular growth, differentiation, embryonic development, and immune response (*38*). These processes are mediated by binding of RA to nuclear transcription factors which, in turn, modulate gene expression. In rhodopsin, crucial for vision, retinal is covalently linked with opsin, a seven-transmembrane helical receptor. The related microbial rhodopsins act as light-driven ion pumps and photosensory pigments. Biochemical data presented here show that RA is a genuine substrate for CYP120A1. On the basis of the RA-bound crystal structure, it seems likely that C2 or methyl groups C16 and C17 become modified by CYP120A1.

Retinoids and their metabolic enzymes have been found in several cyanobacteria. An all-*trans*-retinal-bound sensory rhodopsin from *Anabaena* shows light-induced changes in its isomeric configuration and may be responsible for ambient light signaling in several physiological processes that depend on light (e.g., chromatic adaptation) (*39*). Several retinal-forming carotenoid oxygenases have recently been identified in cyanobacteria, including NosACO from *Anabaena* (*Nostoc* sp. PCC 7120) and Diox1 from *Synechocystis* sp. PCC 6803 (*40, 41*). These discoveries strongly suggest that retinoids and other carotenoid derivatives are physiologically important for cyanobacteria and that enzymes involved in their modification and degradation are essential for normal photosynthetic growth.

The fact that all-*trans*-retinoic acid binds to CYP120A1 protein at micromolar concentrations generating typical type I binding spectra suggests that it is one of these enzymes. The observation that a polar product is generated by CYP120A1 action on retinoic acid in the presence of *Synechocystis* cellular proteins (see the Supporting Information) suggests that it is responsible for hydroxylation of one or more of the retinoic acid and retinal derivatives.

The genome of *Synechocystis* sp. PCC 6803 was published 11 years ago (*42*). It is striking that immediately downstream of the CYP120A1 gene (slr0574) is an open reading frame (slr0575) encoding a 184-residue protein of unknown function. This putative protein is 37% identical in sequence with the *Arabidopsis thaliana* APE1 protein that, when mutated, results in plants that are much slower in adjusting their thylakoid membrane composition in response to changing light conditions (*43*). The neighborhood of these two genes provides an intriguing link between CYP120A1 and photosynthesis that will be the subject of future analysis.

ACKNOWLEDGMENT

We thank Anna Scherer for advice on crystallization, Elisabeth Hartmann for measurement of spectra, Dr. Robert L. Shoeman for performing mass spectrometric analysis, and Dr. Tatiana Domratcheva for the calculation of the carotene coordinates. Diffraction data were collected at beamline X10SA (Swiss Light Source, Paul Scherrer Institute, Villigen, Switzerland). We thank Dr. Ehmke Pohl and Dr. Anuschka Pauluhn for their support in setting up the beamline and are grateful to Dr. Ingrid Vetter for support of the crystallographic software. We also acknowledge Dr. Jerome Baudry for the molecular docking of retinoids in the CYP120A1 crystal structure.

SUPPORTING INFORMATION AVAILABLE

Metabolism of [^{3}H]retinoic acid by CYP120A1 using *Synechocystis* cell lysates analyzed by TLC (Figures S1−S3) and 13-*cis*-β-carotene binding of CYP120A1 probed spectroscopically (Figure S4). This material is available free of charge via the Internet at http://pubs.acs.org.

REFERENCES

1. Mansuy, D. (1998) The great diversity of reactions catalyzed by cytochromes P450. *Comp. Biochem. Physiol., Part C: Pharmacol., Toxicol. Endocrinol. 121*, 5–14.
2. Ortiz de Montellano, P. R. (2005) *Cytochrome P450: Structure, Mechanism and Biochemistry*, Kluwer Academic/Plenum Publishers, New York.
3. Denisov, I. G., Makris, T. M., Sligar, S. G., and Schlichting, I. (2005) Structure and chemistry of cytochrome P450. *Chem. Rev. 105*, 2253–2277.
4. Sigel, A., Sigel, H., and Sigel, R. K. O. (2007) *The Ubiquitous Roles of Cytochrome P450 Proteins*, John Wiley & Sons, Ltd., Chichester, U.K.
5. Werck-Reichhart, D., and Feyereisen, R. (2000) Cytochromes P450: A success story. *Genome Biol. 1*, REVIEWS3003.
6. Feyereisen, R. (2005) Insect cytochrome P450, in *Comprehensive Molecular Insect Science* (Gilbert, L. I., Latrou, K., and Gill, S. S., Eds.) pp 1−77, Elsevier, Oxford, U.K.
7. Kelly, S. L., Kelly, D. E., Jackson, C. J., Warrilow, A. G. S., and Lamb, D. C. (2005) The diversity and importance of microbial cytochromes P450, in *Cytochrome P450: Structure, Mechanism and Biochemistry* (Ortiz de Montellano, P. R., Ed.) 3rd ed., Kluwer Academic/Plenum Publishers, New York.
8. Guengerich, F. P. (2006) Cytochrome P450s and other enzymes in drug metabolism and toxicity. *AAPS J. 8*, E101–E111.
9. Schuler, M. A., Duan, H., Bilgin, M., and Ali, S. (2006) *Arabidopsis* P450s through the looking glass: A window on plant biochemistry. *Phytochem. Rev. 5*, 205–237.
10. Baudry, J., Rupasinghe, S., and Schuler, M. A. (2006) Class-dependent sequence alignment strategy improves the structural and functional modeling of P450s. *Protein Eng., Des. Sel. 19*, 345–353.
11. Rupasinghe, S., and Schuler, M. A. (2006) Homology modeling of plant P450s. *Phytochem. Rev. 5*, 473–505.
12. Ke, N., Baudry, J., Makris, T. M., Schuler, M. A., and Sligar, S. G. (2005) A retinoic acid binding cytochrome P450: CYP120A1 from *Synechocystis* sp. PCC 6803. *Arch. Biochem. Biophys. 436*, 110–120.
13. Segel, I. H. (1975) *Enzyme Kinetics: Behavior and Analysis of Rapid Equilibrium and Steady-State Enzyme Systems*, John Wiley & Sons, Inc., New York.
14. Van Duyne, G. D., Standaert, R. F., Karplus, P. A., Schreiber, S. L., and Clardy, J. (1993) Atomic structures of the human immunophilin FKBP-12 complexes with FK506 and rapamycin. *J. Mol. Biol. 229*, 105–124.
15. Kabsch, W. (1993) Automatic Processing of Rotation Diffraction Data from Crystals of Initially Unknown Symmetry and Cell Constants. *J. Appl. Crystallogr. 26*, 795–800.
16. Pape, T., and Schneider, T. R. (2004) HKL2MAP: A graphical user interface for phasing with SHELX programs. *J. Appl. Crystallogr. 37*, 843–844.
17. de La Fortelle, E., and Bricogne, E. (1997) Maximum-Likelihood Heavy-Atom Parameter Refinement for the Multiple Isomorphous Replacement and Multiwavelength Anomalous Diffraction Methods. *Methods Enzymol. 276*, 472–494.
18. Terwilliger, T. C. (2000) Maximum-likelihood density modification. *Acta Crystallogr. D56*, 965–972.
19. Emsley, P., and Cowtan, K. (2004) Coot: Model-building tools for molecular graphics. *Acta Crystallogr. D60*, 2126–2132.
20. Murshudov, G. N., Vagin, A. A., and Dodson, E. J. (1997) Refinement of macromolecular structures by the maximum-likelihood method. *Acta Crystallogr. D53*, 240–255.
21. French, S., and Wilson, K. S. (1978) On the Treatment of Negative Intensity Observations. *Acta Crystallogr. A34*, 517–525.

22. Collaborative Computational Project, Number 4 (1994) The CCP4 Suite. Programs for Protein Crystallography. *Acta Crystallogr. D50*, 760–763.
23. Vagin, A. A., and Teplyakov, A. (1997) MOLREP: An automated program for molecular replacement. *J. Appl. Crystallogr. 30*, 1022–1025.
24. Domanski, T. L., and Halpert, J. R. (2001) Analysis of mammalian cytochrome P450 structure and function by site-directed mutagenesis. *Curr. Drug Metab. 2*, 117–137.
25. Poulos, T. L., and Meharenna, Y. T. (2007) Structures of P450 Proteins and Their Molecular Phylogeny, in *The Ubiquitous Roles of Cytochrome P450 Proteins* (Sigel, A., Sigel, H., and Sigel, R. K. O., Eds.) pp 57−96, John Wiley & Sons, Ltd., Chichester, U.K.
26. von König, K., and Schlichting, I. (2007) Cytochromes P450 Structural Basis for Binding and Catalysis, in *The Ubiquitous Roles of Cytochrome P450 Proteins* (Sigel, A., Sigel, H., and Sigel, R. K. O., Eds.) Metal Ions in Life Sciences Edition, pp 235−265, John Wiley & Sons, Ltd., Chichester, U.K.
27. Beitlich, T., Kühnel, K., Schulze-Briese, C., Shoeman, R. L., and Schlichting, I. (2007) Cryoradiolytic reduction of crystalline heme proteins: Analysis by UV-vis spectroscopy and X-ray crystallography. *J. Synchrotron Radiat. 14*, 11–23.
28. Holm, L., and Sander, C. (1993) Protein structure comparison by alignment of distance matrices. *J. Mol. Biol. 233*, 123–138.
29. Ravichandran, K. G., Boddupalli, S. S., Hasermann, C. A., Peterson, J. A., and Deisenhofer, J. (1993) Crystal structure of hemoprotein domain of P450BM-3, a prototype for microsomal P450's. *Science 261*, 731–736.
30. Lee, D. S., Yamada, A., Sugimoto, H., Matsunaga, I., Ogura, H., Ichihara, K., Adachi, S., Park, S. Y., and Shiro, Y. (2003) Substrate recognition and molecular mechanism of fatty acid hydroxylation by cytochrome P450 from *Bacillus subtilis*. Crystallographic, spectroscopic, and mutational studies. *J. Biol. Chem. 278*, 9761–9767.
31. Haines, D. C., Tomchick, D. R., Machius, M., and Peterson, J. A. (2001) Pivotal role of water in the mechanism of P450BM-3. *Biochemistry 40*, 13456–13465.
32. Gotoh, O. (1992) Substrate recognition sites in cytochrome P450 family 2 (CYP2) proteins inferred from comparative analyses of amino acid and coding nucleotide sequences. *J. Biol. Chem. 267*, 83–90.
33. Poulos, T. L., Finzel, B. C., and Howard, A. J. (1987) High-resolution crystal structure of cytochrome P450cam. *J. Mol. Biol. 195*, 687–700.
34. Cupp-Vickery, J. R., and Poulos, T. L. (1995) Structure of cytochrome P450eryF involved in erythromycin biosynthesis. *Nat. Struct. Biol. 2*, 144–153.
35. Nagano, S., Li, H., Shimizu, H., Nishida, C., Ogura, H., Ortiz de Montellano, P. R., and Poulos, T. L. (2003) Crystal structures of epothilone D-bound, epothilone B-bound, and substrate-free forms of cytochrome P450epoK. *J. Biol. Chem. 278*, 44886–44893.
36. Schlichting, I., Berendzen, J., Chu, K., Stock, A. M., Maves, S. A., Benson, D. E., Sweet, R. M., Ringe, D., Petsko, G. A., and Sligar, S. G. (2000) The catalytic pathway of cytochrome p450cam at atomic resolution. *Science 287*, 1615–1622.
37. Fedorov, R., Ghosh, D. K., and Schlichting, I. (2003) Crystal structures of cyanide complexes of P450cam and the oxygenase domain of inducible nitric oxide synthase-structural models of the short-lived oxygen complexes. *Arch. Biochem. Biophys. 409*, 25–31.
38. Blomhoff, R., and Blomhoff, H. K. (2006) Overview of retinoid metabolism and function. *J. Neurobiol. 66*, 606–630.
39. Vogeley, L., Sineshchekov, O. A., Trivedi, V. D., Sasaki, J., Spudich, J. L., and Luecke, H. (2004) *Anabaena* sensory rhodopsin: A photochromic color 0 sensor at 2.0 Å. *Science 306*, 1390–1393.
40. Ruch, S., Beyer, P., Ernst, H., and Al-Babili, S. (2005) Retinal biosynthesis in Eubacteria: In vitro characterization of a novel carotenoid oxygenase from *Synechocystis* sp. PCC 6803. *Mol. Microbiol. 55*, 1015–1024.
41. Scherzinger, D., Ruch, S., Kloer, D. P., Wilde, A., and Al-Babili, S. (2006) Retinal is formed from apo-carotenoids in *Nostoc* sp. PCC7120: In vitro characterization of an apo-carotenoid oxygenase. *Biochem. J. 398*, 361–369.
42. Kaneko, T., and Tabata, S. (1997) Complete genome structure of the unicellular cyanobacterium *Synechocystis* sp. PCC6803. *Plant Cell Physiol. 38*, 1171–1176.
43. Walters, R. G., Shephard, F., Rogers, J. J., Rolfe, S. A., and Horton, P. (2003) Identification of mutants of *Arabidopsis* defective in acclimation of photosynthesis to the light environment. *Plant Physiol. 131*, 472–481.
44. Wallace, A. C., Laskowski, R. A., and Thornton, J. M. (1995) LIGPLOT: A program to generate schematic diagrams of protein-ligand interactions. *Protein Eng. 8*, 127–134.

BI800328S